Wind and Structures, *Vol. 23, No. 4 (2016) 301-311*
DOI: http://dx.doi.org/10.12989/was.2016.23.4.301

Numerical simulation for unsteady flow over marine current turbine rotors

A. Reza Hassanzadeh [*1], Omar bin Yaakob[1,2a],
Yasser M. Ahmed[1,3b] and M. Arif Ismail[1c]

[1]*Faculty of Mechanical Engineering, Universiti Teknologi Malaysia, 81310, Skudai, Johor, Malaysia*
[2]*Marine Technology Centre, Universiti Teknologi Malaysia, 81310, Skudai, Johor, Malaysia*
[3]*Faculty of Engineering, Alexandria University, Egypt*

(Received September 16, 2015, Revised June 27, 2016, Accepted June 28, 2016)

Abstract. The numerous benefits of Savonius turbine such as simple in structure, has appropriate self-start ability, relatively low operating velocity, water acceptance from any direction and low environmental impact have generated interests among researchers. However, it suffers from a lower efficiency compared to other types of water turbine. To improve its performance, parameters such flow pattern, pressure and velocity in different conditions must be analyzed. For this purpose, a detailed description on the flow field of various types of Savonius rotors is required. This article presents a numerical study on a nonlinear two-dimensional flow over a classic Savonius type rotor and a Benesh type rotor. In this experiment, sliding mesh was used for solving the motion of the bucket. The unsteady Reynolds averaged Navier-Stokes equations were solved for velocity and pressure coupling by using the SIMPLE (Semi-Implicit Method for Pressure linked Equations) algorithm. Other than that, the turbulence model using k-ε standard obtained good results. This simulation demonstrated the method of the flow field characteristics, the behavior of velocity vectors and pressure distribution contours in and around the areas of the bucket.

Keywords: CFD; angle of attack; turbulence model; structure of profile

1. Introduction

Currently, the interest and demand regarding renewable energy is growing. Ocean energy is a huge resource of renewable energy, which encompasses 70% of the planet Earth. One source of ocean energy is ocean current. Though surrounded by sea, the ocean current velocity in Malaysian sea is low (around 0.56 m/s), and water level is relatively shallow (Yaakob *et al.* 2010, Chong and Lam 2013). There are two types of turbine used to harvest energy from current, which are horizontal axis marine current turbine (HAMCT) (Thomas 2007 and Yi *et al*. 2014) and vertical axis marine current turbine (VAMCT). Savonius type turbines, originally developed for wind

∗Corresponding author, Ph.D., E-mail: rhm1425@gmail.com
[a] Professor., E-mail: Omar@fkm.utm.my
[b] Ph.D., E-mail: Yasser@mail.fkm.utm.my
[c] Ph.D. Student, E-mail: Mohd-arif.ismail@yahoo.com

http://www.techno-press.org/?journal=was&subpage=8 ISSN: 1226-6116 (Print), 1598-6225 (Online)

energy applications are found to be suitable for low-speed current flow. (Yaakob 2006, Alam 2009, Aresti *et al.* 2013 and Zamani *et al.* 2016).

The conventional Savonius turbine has low efficiency and negative torque, especially at angles of 135° to 165° and from 315° to 345° (Kamoji *et al.* 2009b). A number of improvement has been proposed, such as addition of the number of blade stages of Savonius to two or three steps, as reported by Khan (2009c) and Nakajima *et al.* (2008). One of the most important issues about turbines is the direct relation between the turbine rotor and the flow pattern. Zhou and Rempfer (2013) used numerical simulation of the flow to study two types of rotor. They were studied to numerically discover the two-dimensional non-linear unsteady flow to evaluate the aerodynamic characteristics and analyze the pressure distribution on the revolving blades.

The aim of this study is to analyze and compare the two types of rotors, which are a Savonius type rotor and a Benesh type rotor. Actually the main originality of the current research paper is survey the effect of renovating Savonius rotor and Benesh type rotor on performance and negative torque and more study about velocity and pressure on the two type of rotors. By using CFD methodology, velocity and pressure distributions were obtained near the rotor blade surface (Unchai and Janyalertadun 2014). Attention was also given to the correction between the rotor performance and flow pattern.

2. Simulation model

For the simulation, two-dimensional designs of the conventional Savonius and Benesh type models were drowned. The designs were saved in IGES format, and then ANSYS ICEM CFD 13.0 was used to create the mesh. Many different models can be used for simulation of turbulence, each having its own benefits. In this study, attention was given to improve rotor performance and flow pattern by using standard k-ε turbulence models because that gave satisfactory results.

2.1 Rotor geometry

Savonius rotor has a "S-shaped" cross section, made up of two semi-circular buckets, based on the Savonius rotor established by Flettner. Meanwhile, Benesh developed two rotors with superior performance in 1987 and 1996 (Akwa *et al.* 2012b).

Fig. 1 displays the characteristic factors of marine current turbine rotor with two buckets of a semi-circular profile, and Benesh profile subjected to a current with water velocity, V_o, and at a rate of rotation represented by ω. The structure of the sample Savonius was driven at rather low speeds, having high static and dynamic moment, and set to be able to accept any current for the operation. Moreover, Light weight material will help reducing dead weight.

The driving force on the buckets of the Savonius acted as drag force, while the lift force functioned to contribute to torque construction at small angles of attack (Manwell *et al.* 2010). The static torque at dissimilar rotor angles was not constant. The helical Savonius has a number of advantages, which makes it appropriate for power generation compared to conventional ones (Grinspan *et al.* 2001 and Hassan 2011)

- The twisted/helical buckets of rotor have tremendous self-start ability.
- Capable to run smoothly at high revolution per minute (RPM) at low fluid velocity.
- Having higher average of power output, and steady operation.

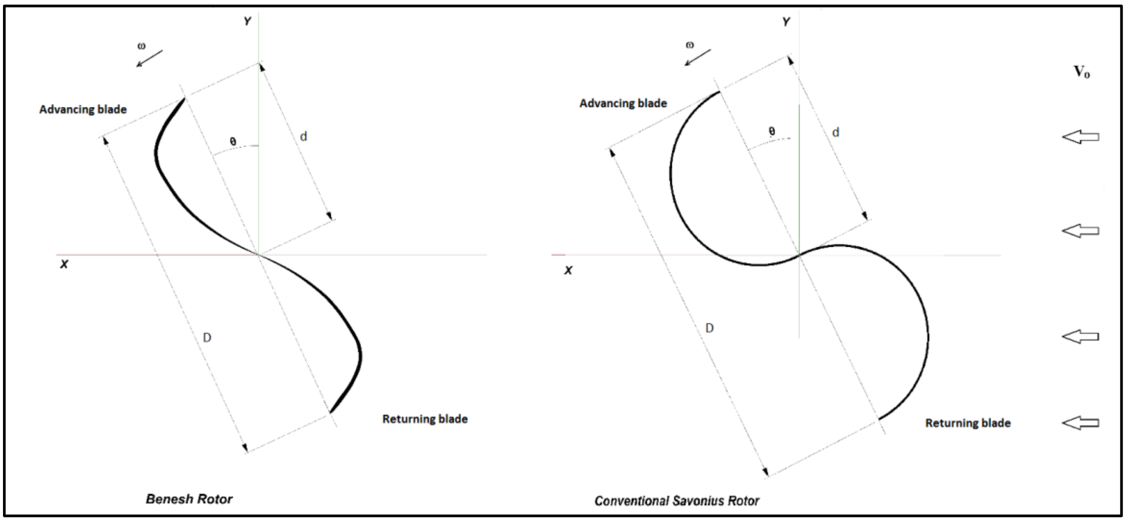

Fig. 1 Schematic representations of conventional Savonius rotor and Benesh rotor

Table 1 Dimensions and Condition for Model Simulation

No.	Specification	Value
1	Diameter of Rotor, D_R	0.75 m
2	Diameter of Paddles, D_B	0.375 m
3	Speed range, V_0	0.177 m/s

Table 1, presents some of the main characteristics of the Savonius turbine.

The CFD simulations were implemented in two stages as follows: firstly is creating two-dimensional mesh for Savonius and Benesh type rotors with two endplates and no central shaft, and secondly, using Fluent software for computing and analyzing the cases. The second set of simulation used 2-D transient computational model with Sliding Mesh Method (SMM). The overall domain was then divided into two sub-domains; a stationary stator domain and another one rotor sub-domain that rotated with respect to the stationary domain. This permitted sliding of the adjacent cells at the boundary between the two sub-domains.

2.2 Mathematical formulation

The available power of the turbine analyzed in the water channel was calculated as

$$P_{available} = 0.5\ \rho A V_o^{3} \tag{1}$$

$P_{available}$ is Power available in water (Watts). In situation where C_p is the power coefficient of the Savonius turbine, the power taken by the turbine would be equal to

$$P = P_{available}\, C_P \tag{2}$$

The power coefficient C_p of a Savonius turbine was calculated using

$$C_p = \frac{\mathrm{P}}{P_{availa}} = \frac{2M\omega}{\rho A V o^3} = \frac{2M}{\rho A V o^2 r}\frac{\omega r}{V_o} = C_M \lambda \tag{3}$$

The area of Savonius rotor was given by

$$A = HD \tag{4}$$

The coefficient of Moment (C_M) was defined as

$$C_M = 2M / (\rho A V o^2 d) \tag{5}$$

where M is Moment and C_M is coefficient of Moment.

The tip speed of the rotor was calculated using

$$U = \omega d \tag{6}$$

The Tip Speed Ratio (TSR) of the turbine is a very significant parameter, given by

$$TSR = \lambda = U / V_o \tag{7}$$

Nonetheless, the solution for the three-dimensional flow was governed the Navier-Stokes equations by an incompressible version for field surrounding the rotating turbine. For that domain, the full Navier-Stokes equations was not considered at this point (Nichols 2010).

$$\nabla \cdot (\vec{v}_r) = 0 \tag{8}$$

$$\rho \nabla \cdot (\vec{v}_r \vec{v}_r) + \rho(2\vec{\omega} \times \vec{v}_r + \vec{\omega} \times \vec{\omega} \times \vec{r}) = -\nabla \mathrm{p} + \nabla \bar{\bar{\tau}}_{\mathrm{r}} + \vec{F} \tag{9}$$

Where ρ is the water density, t is time, $\vec{v}_r$ represents the relative velocity vector observed from the revolving rotational domain, $\vec{\omega}$ is the angular velocity vector relative to the stationary domain, $\vec{r}$ shows the position vector from the origin, p is the fluid pressure, $\bar{\bar{\tau}}$ represents the viscous stress tensor, and $\vec{F}$ shows the gravitational force vector. There are two terms for acceleration in the moment equation to define the marine current rotation, which are the centripetal acceleration ($\vec{\omega} \times \vec{\omega} \times \vec{r}$) and the Coriolis acceleration ($2\vec{\omega} \times \vec{v}_r$).

Turbulence can be simulated using many different models; each has its own advantages. The mathematical equations of the standard k-ε turbulence model used in this study were as follows (Launder and Spalding 1974)

$$v_t = c_\mu \frac{k^2}{\epsilon} \tag{10}$$

$$\left(\frac{\partial(\rho k)}{\partial t} + U_j \frac{\partial(\rho k)}{\partial x_j}\right) = P^{(k)} - \rho\epsilon + \frac{\partial}{\partial x_j}[(\mu + \sigma_\epsilon \mu_t)\frac{\partial k}{\partial x_j}] \tag{11}$$

$$\left(\frac{\partial(\rho \epsilon)}{\partial t} + U_j \frac{\partial(\rho \epsilon)}{\partial x_j}\right) = C_{\epsilon 1}\frac{\epsilon}{k}P^{(k)} - C_{\epsilon 2}\rho\frac{\epsilon^2}{k} + \frac{\partial}{\partial x_j}[(\mu + \sigma_\epsilon \mu_t)\frac{\partial \epsilon}{\partial x_j}] \tag{12}$$

For determining the turbulent viscosity, Eq. (13) was used in the model in low Reynolds numbers. However, in order to handle high Reynolds numbers, Eq. (14) was integrated following the standard k-ε turbulence formulation of the turbulent viscosity.

$$d\left(\frac{\rho^2 k}{\sqrt[2]{\in\mu}}\right) = 1.72\frac{\hat{v}}{\sqrt[2]{\hat{v}^3-1+c_v}}d\hat{v} \tag{13}$$

where, $\hat{v} = \frac{\mu_{eff}}{\mu}$ and $c_v \approx 100$.

$$\mu_t = \rho c_\mu \frac{k^2}{\epsilon} \tag{14}$$

where, $c_\mu = 0.0845$.

2.3 Turbulence modeling

An important parameter for simulation is flow separation, which can affect the efficiency of the turbine. It is also necessary to follow accurate CFD procedure to simulate real conditions. By using the SIMPLE (Semi-Implicit Method for Pressure linked Equations) algorithm, the unsteady Reynolds averaged Navier-Stokes equations were solved for velocity and pressure coupling.

A two-dimensional design of the conventional Savonius and Benesh type models were created using Rhinoceros software. The designs were saved in IGES format, and then ANSYS ICEM CFD 13.0 was used to develop the mesh.

In this study, ANSYS Fluent 13.0 code was applied for simulation and analysis. The unstructured mesh element number used for the Benesh type rotor and Savonius rotor was around 950,000.

Fig. 2 shows the computational domain and the unstructured mesh grid for the rotor geometry. The inlet and outflow situations were observed from the right and left boundaries condition individually. The buckets and plates were fixed to the standard wall. The velocity of water was 0.177 m/s in the inlet. In order to control the separated rotor wakes, the density of mesh was increased near the bucket margins, tips, which then declined away from the rotor.

According to Mohamed *et al.* (2010) and Gupta and Sharma (2011), one of the best turbulence models that an outstanding contract between the CFD and experimental is the standard k-ε turbulence model for goal function, C_p (incomprehensible). In this study, this model was used for running the application.

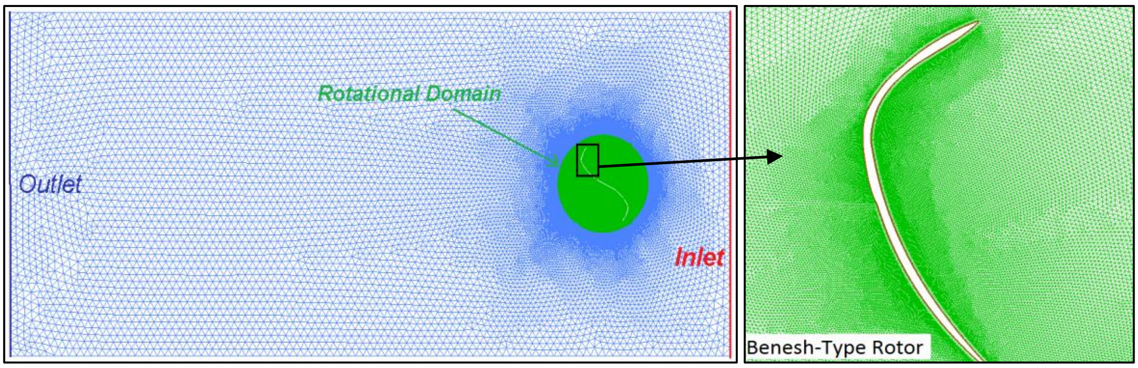

Fig. 2 (a) Computational domain and boundary condition and (b) Unstructured mesh of Benesh type rotor

According to Yaakob *et al.* (2012) and Reza Hassanzadeh *et al.* (2013), the second-order upwind numerical scheme gives more accurate results. Therefore, the second-order upwind numerical scheme was chosen for the calculation in this study. Amongst the chosen CFD trial cases, the standard k-ε turbulence model has proper performance for relativity simple geometries for the same channel flow pipe.

3. Results and discussion

When the fluid motion is acceptable, it will enter as force on the fluid, which can be decomposed into two forces. One force will be in the direction of the fluid velocity, and the other in perpendicular direction. Force in the direction of water flow is called drag force, while the one perpendicular to its direction is known as lift force. Drag force has deterrent on the fluid motion around the object, while the nature of the lift force is lifting. Rotation of the Savonius blades (vertical axis) will create fluid drag. Unlike vertical axis turbine blades, the torque required to rotate the horizontal axis turbine blades is the lift force.

As shown in Figs. 3 and 4, the velocity at the back of the advancing blade was improved. Analysis on the contour plot revealed the physical flow of a marine current turbine rotor and its mechanism of energy generation. The relative velocity vectors showed that the velocity vector was directed from the inside to the downstream side of the rotor.

As displayed in the figures, the highest speed occurred at the edge of the turbine bucket. As shown in Fig. 3, it was clear that there were two branches of vortices created at the blades. One collection was produced at the upper tip and the lower tip of the Savonius rotor, and also at downstream of the flow of the Benesh type rotor, in which these vortices revolved counterclockwise. This kind of vortex was the reason for the reduction of torque and increment of the power of the suction pressure on the convex side of the blades. Moreover, high velocity areas are more pronounced at the leading edge of Benesh than the Savonius rotor.

The further collection can be divided into two groups; one created along the upstream of the flow of the returning and another on advancing blades. The vortices on the Benesh type rotor were bigger than those on the Savonius rotor, and there were two separate points on the Savonius rotor. In different rotation angles, the influence of vortices was dissimilar.

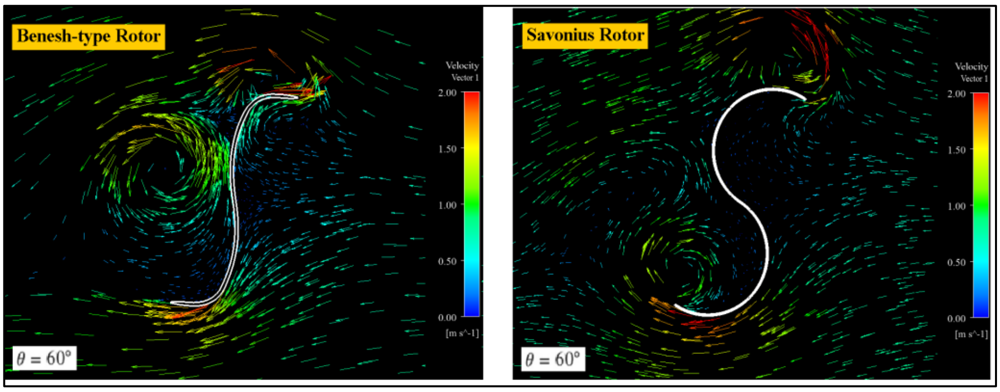

Fig. 3 Vector of velocity around rotors at 60o of attack

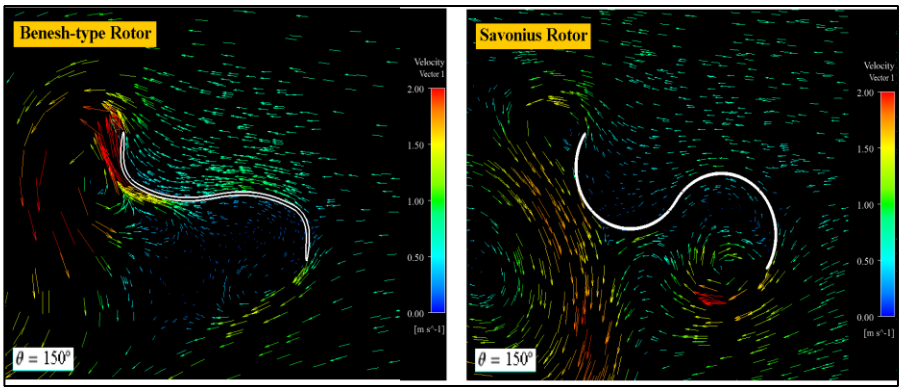

Fig. 4 Vector of velocity around rotors at 150^{o} of attack

As described, the flow speed of the rotor was at the bucket concave. Due to pressure, the rotation of the rotor faced pressure. Correspondingly, this was true for the Benesh type rotor. Due to the structure of the blade, it could rotate easier. The static pressure contours from unsteady two-dimensional simulations were then analyzed to explain the torque production mechanisms of the Savonius under unsteady situations.

As can be seen in Fig. 5, pressure contours on the rotor occurred at three different angles of attack. At the angle of attack of 30°, in comparison with Savonius rotor, Benesh type rotor was found to gain more pressure on the convex of the advancing blade and near the center of the blades, which created more torque. It was also observed that there was a negative pressure at the center of the Savonius rotor.

At the angle of attack of 90° as shown in the same figure, the same semi-circular design Savonius rotor was able to absorb more pressure on the convex of the advancing blade of the water flow compared to that on Benesh type, and had more areas to generate higher pressure. At this angle of attack, the area with a negative pressure in the upstream was rarely seen, unlike in the downstream, where there was considerable negative pressure.

As can be understood in Figs. 3 and 4, the eddies at the tip are more pronounced in the Savonius rotor than the Benesh at 60˚at both edges; however, it is not the case at 150°. This aspect show that maximum speed of the water flow in opposite direction is at 60˚ at the top. It is more in case of Savonius rotor as compared to Benesh.

However, naturally, the angle of attack of the rotor at 150°, maximum pressure value could be seen both on the concavity of the returning blades, because the direction of the blades was opposite to the direction of the marine current. Note that in Fig. 5, the Benesh type design created proper pressure at this angle, on the convex of the advancing blade. Another point of consideration at this angle of attack was the negative pressure on the concave of the advancing blade, in which it appeared as a negative pressure of the Benesh type rotor, more than that on the Savonius rotor.

On the other hand, for the flow configuration of study, with regard to the acting on the velocity, the maximum and minimum pressure of the rotor are important as the optimization step to obtain a better understanding on the operating principle for different rotors.

As described, it was also observed that there were negative pressure and negative torque, Whereas, Negative torque might be reduced if 3 blades are tested instead of two, in future, various simulations will be performed for the model 3-blade combination as well.

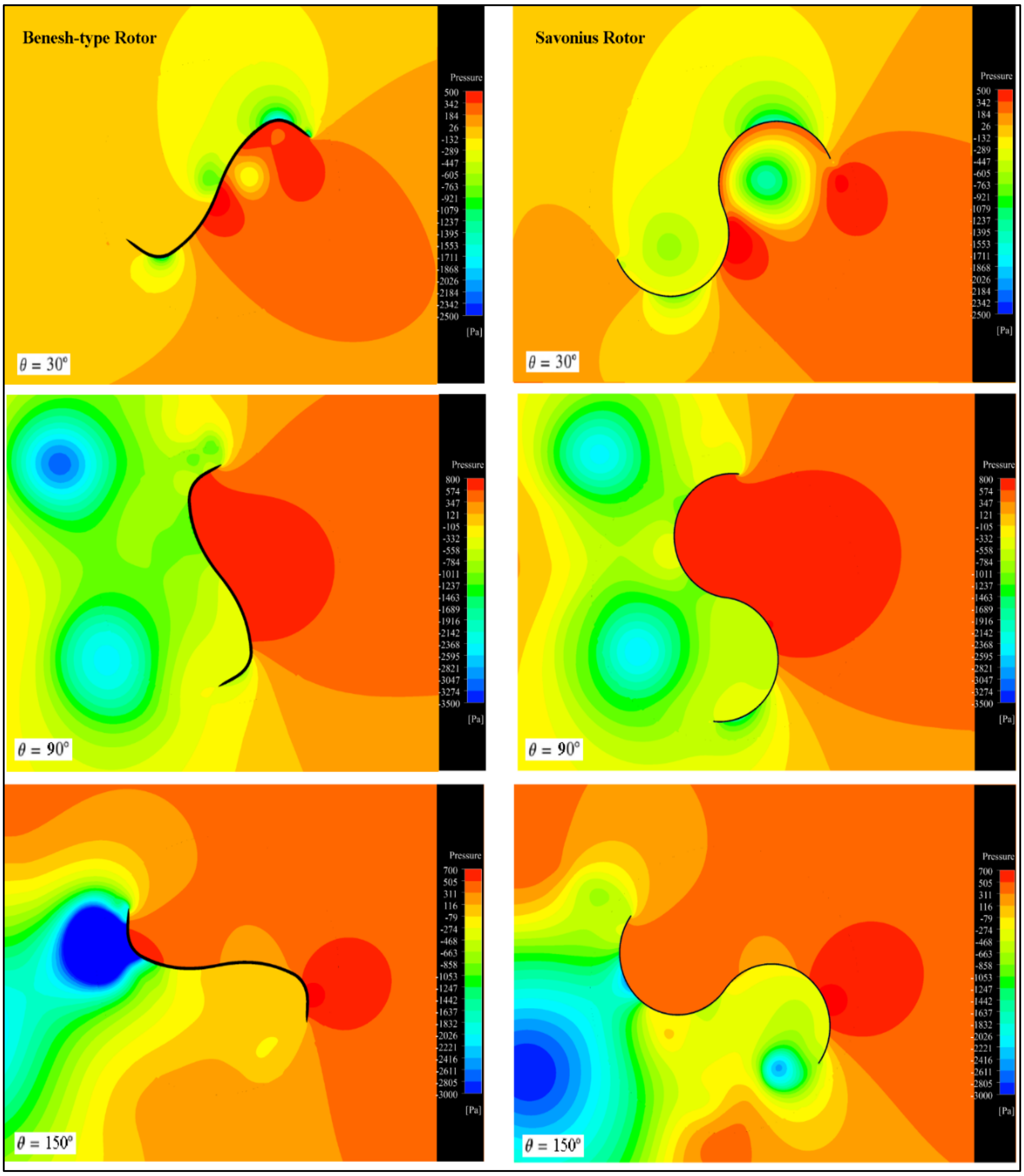

Fig. 5 Static pressure contours around rotors at different angle of attack

4. Conclusions

The main aim of this study was to predict the flow behavior around Savonius-type turbines by using a simulation method. The other purpose of the current study was to compare two types of turbines, which are the conventional Savonius turbine and Benesh type turbines. The standard k-ε turbulence model, as well as the simulation scheme in second order for the finite volume solver, was used to increase the accuracy.

Detailed velocity vectors and pressure distribution were studied and analysed to characterise the differences between these kinds of rotors, in terms of their performance. The results show that an open (elliptical) blade is better than closed (circular) blade in the marine conditions.

Acknowledgments

The authors would like to express gratitude to Universiti Teknologi Malaysia (UTM) and the Ministry of Higher Education (MOHE) for funding this project under the Exploratory Research Grant Scheme Vote No: 4L125.

References

Akwa, J.V., Vielmo, H.A. and Petry, A.P. (2012b), "A review on the performance of savonius wind turbines", *Renew. Sust. Energ. Rev.*, **16**(5), 3054-3064.

Alam, M.D.J. (2009), *Design and Development of a Marine Current Energy Conversion System Using Hybrid Vertical Axis Turbine*, Master. Memorial university of Newfoundland.

Aresti, L., Tutar, M., Chen, Y. and Calay, R.K. (2013), "Computational study of a small scale vertical axis wind turbine (VAWT): comparative performance of various turbulence models", *Wind Struct.*, **17**(6), 647-670.

Chong, H.Y. and Lam, W.H. (2013), "Ocean renewable energy in Malaysia: The potential of the straits of malacca", *Renew. Sust. Energ. Rev.*, 23, 169-178.

Grinspan, A., Kumar, P.S., Saha, U., Mahanta, P., Rao, D.V.R. and Bhanu, G.V. (2001), "Design, development and testing of Savonius wind turbine rotor with twisted blades. Department of Mechanical Engineering", *Indian Institute of Technology,Guwahati, India*.

Gupta, R. and Sharma, K.K. (2011), "Flow physics of a three-bucket savonius rotor using Computational Fluid Dynamics (CFD)", *IJRMET*, **1**(1).

Hassan, M. (2011), *Twisted Savonius turbine based marine current energy conversion system*, Memorial University of Newfoundland (Canada): ProQuest Dissertations And Theses.

Hassanzadeh, A.R., Yaakob, O., Ahmed, Y.M. and Ismail, M.A. (2013), "Comparison of conventional and helical savonius marine current turbine using computational fluid dynamics", *World Appl. Sci. J.*, **28**(8), 1113-1119.

Kamoji, M., Kedare, S. and Prabhu, S. (2009b), "Performance tests on helical Savonius rotors", *Renew. Energy*, **34**(3), 521-529.

Khan, J. and Bhuyan, G.S. (2009a), Ocean Energy: Global Technology Development Status, *IEA-OES. Document* (T0104).

Khan, N.I., Iqbal, T., Hinchey, M. and Masek, V. (2009c), "Performance of savonius rotor as a water current turbine", *J. Ocean Technol*., **4**(2), 71-83.

Launder, B.E. and Spalding, D. (1974), "The numerical computation of turbulent flows", *Comput. Method. Appl. Mech. Eng*., **3**(2), 269-289.

Manwell, J.F., McGowan, J.G. and Rogers, A.L. (2010), *Wind energy explained: theory, design and application*, John Wiley & Sons.
Mohamed, M.H., Janiga, G., Pap, E. and Thévenin, D. (2010), "Optimization of Savonius turbines using an obstacle shielding the returning blade", *Renew. Energy*, **35**(11), 2618-2626.
Nakajima, M., Iio, S. and Ikeda, T. (2008), "Performance of double-step savonius rotor for environmentally friendly hydraulic turbine", *J. Fluid Sci. Technol.*, **3**(3), 410-419.
Nicholson, K.M. (2010), *Numerical investigation of the aerodynamic performance of a double-stage savonius rotor with twisted blades*, Master of science. University of Louisville
Thomas, K. (2007), Low speed energy conversion from marine currents, Uppsala University
Unchai, T. and Janyalertadun, A. (2014). "CFD evaluation of a suitable site for a wind turbine on a trapezoid shaped hill", *Wind Struct.*, **19**(1), 75-88.
Yaakob, O., Ahmed, Y.M. and Ismail, M.A. (2012), "Validation study for savonius vertical axis marine current turbine using CFD simulation", *Proceedings of the 6th Asia-Pacific workshop on marine hydrodynamics-APHydro2012*.
Yaakob, O., Ariff, M.A.R. and Afifi, M.A.A (2006), "Prospects for Ocean Energy in Malaysia", *Proceedings of the International Conference on Energy and the Environment*, Kuala Lumpur, Malaysia: 28-30.
Yaakob, O., Tawi, K. and Suprayogi, D. (2008b), "Development of vertical axis marine current turbine rotor", *Proceedings of the International Conference Marine Renewable Energy* RINA, London, UK.
Yaakob, O.B., Tawi, K. and Sunanto, D.S. (2010), "Computer simulation studies on the effect overlap ratio for savonius type vertical axis marine current turbine", *Int. J. Eng. Trans. A Basics*, **23**, 79-88.
Yi, J.H., Yoon, G.L. and Li, Y. (2014), "Numerical investigation on effects of rotor control strategy and wind data on optimal wind turbine blade shape", *Wind Struct.*, **18**(2), 195-213.
Zamani, M., Maghrebi, M.J. and Moshizi, S.A. (2016), "Numerical study of airfoil thickness effects on the performance of J-shaped straight blade vertical axis wind turbine", *Wind Struct.*, **22**(5), 595-616.
Zhou, T. and Rempfer, D. (2013), "Numerical study of detailed flow field and performance of Savonius wind turbines", *Renew. Energy*, **51**, 373-381.

CC

Nomenclature

A	projected area of rotor (m^2)
H	length of rotor (m)
D_B	chord of blade (m)
D_R	diameter of rotor (m)
r	radius of the rotor (m)
C	overlap of blades (m)
P	power output from rotor (W)
$P_{available}$	power available output of rotor (W)
M	torque experienced by rotor (N · m)
Vo	water velocity (m/s)
U	rotor tip speed (m/s)
C_P*	power coefficient
C_m*	coefficient of torque
Re*	Reynolds number

Greek letters

λ*	tip speed ratio
α *	aspect ratio
β *	overlap ratio
θ	angle of blade chord (deg.)
ρ	water density (kg/m^3)
ω	angular velocity of rotor (rad/s)

Superscript

*	non-dimensional